Bachelor Project

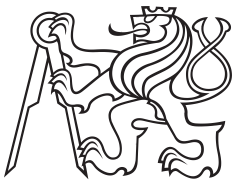

Czech Technical University in Prague

F3

Faculty of Electrical Engineering
Department of Electromagnetic Field

# Optimal Quality Factor of Air Cored Inductors

**Jakub Liška**

Supervisor: doc. Ing. Lukáš Jelínek, Ph.D.
Supervisor–specialist: doc. Ing. Miloslav Čapek, Ph.D.
Field of study: Open Electronic Systems
Subfield: Open Electronic Systems
May 2019

# Acknowledgements

I would like to thank Lukáš Jelínek for an excellent management of this thesis, perfect cooperation, kindliness and provided expertise. I would also like to thank Miloslav Čapek for helpful remarks on this text and assistance in programming problems Vít Losenický for getting me acquainted with AToM and Vojtěch Neuman for providing me a code exporting triangular mesh to TikZ. Furthermore, thanks go to my family and friends for expressing their support and creating a nice environment not only during the process of writing, but also during the whole period of my studies.


# Declaration

I declare that I completed the presented thesis independently and that all used sources are quoted in accordance with the Methodological instructions that cover the ethical principles for writing an academic thesis.

In Prague, 24. May 2019

„Prohlašuji, že jsem předloženou práci vypracoval samostatně, a že jsem uvedl veškeré použité informační zdroje v souladu s Metodickým pokynem o dodržování etických principů při přípravě vysokoškolských závěrečných prací.“

V Praze, 24. květen 2019

# Abstract

The thesis deals with quality factor of air cored inductors and its geometric dependence. The aim is to get acquainted with the given issue and subsequent implementation in AToM with available matrix operators.
All calculations are done for inductors formed by a well conducting strips in vacuum with a focus on canonical structures such as planar spiral, cylindrical helix, spherical helix, and toroidal helix.
Triangular meshes of all these structures have been created by a code developed as a part of this thesis.
Fundamental bounds on quality factor of an inductor has also been evaluated for current supports in a shape of a disc, square, cylinder, sphere, and torus.
Finally, a comparison of a fundamental bound to quality factor and of quality factors of realistic inductors is provided which allowed to mutually compare quality of different inductor designs and opened several questions for further study.



**Keywords:** air cored inductor, optimal, quality factor, triangular mesh



**Supervisor:** doc. Ing. Lukáš Jelínek, Ph.D.
Faculty of Electrical Engineering,
Czech Technical University in Prague,
Technická 1902/2,
Praha 6



# Abstrakt

Práce se zabývá problematikou činitel jakosti induktorů se vzdušným jádrem v závislosti na jejich geometrii. Cílem je seznámení se s danou problematiokou a následnou implementací v nástroji AToM s pomocí dostupných maticových operátorů.
Všechny výpočty jsou provedeny pro induktory tvořené dobře vodivými pásky ve vakuu se zaměřením na kanonické struktury jako jsou planární spirála, cylindrická šroubovice, sférická šroubovice a toroidní šroubovice.
Triangulární mřížky pro všechny tyto struktury byly vytvořeny pomocí kódu vyvinutého jako součást této práce.
Fundamentální limit činitele jakosti induktoru byl nalezen pro oblast proudu na disku, čtvercové desce, válci, kouli a torusu.
Na závěr bylo provedeno porovnání fundamentálního limitu čuinitele jakosti a činitelů jakosti skutečných induktorů, což dovolilo vzájemné porovnat jakosti induktorů o rozličných tvarech a otevřelo spoustu otázek pro další zkoumání.



**Klíčová slova:** induktor s vzdušným jádrem, optimální, činitel jakosti, triangulární mřížka

**Překlad názvu:** Optimální činitel jakosti induktoru se vzdušným jádrem

# Contents

# Figures

# Tables

# Chapter 1

# Introduction

An inductor is a passive circuit element designed to store magnetic energy [1]. *Coil* and *choke* are terms, which are also used for inductors [1]. For this property this circuit element is widely used throughout the electrical engineering, most notable examples being power supplies, transformers, radios, TVs, and electric motors.

In principle, any electric current flowing in a conductor evince inductive properties, meaning that if electromagnetic field generated by such current exhibits an excess in magnetic energy, it can be considered as *inductor*. However, practical inductors are usually formed into helix or spiral [1, 2], which at low electrical sizes greatly reduce the electric energy storage. Cylindrical helix and toroidal helix are the most typical shapes 1.1.

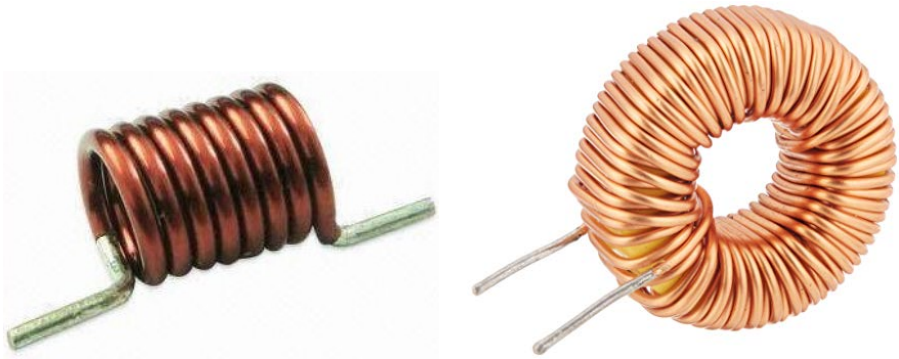

**(a) :** Solenoid [3]. **(b) :** Toroid [4].

**Figure 1.1:** Typical shapes of inductors.

The most important quantity describing an inductor is inductance which is a constant of proportionality between voltage across the inductor and the time rate of change of the current [5, 2]. The unit of inductance is henry (H), named in honor of the famous American inventor Joseph Henry, who discovered inductance and constructed an electric motor. His discovery of electromagnetic induction was made before Faraday, but Henry failed to publish his findings [1, 2].

The inductance depends on inductor's dimensions, construction and operational frequency. The inductance is also commonly modified by introduction of magnetic materials, this thesis is however solely focused on air cored inductors. Without magnetic material, the inductance values of practical inductors range from a few microhenrys, as in communication systems, to tents of milihenrys, as in power systems [1, 2].

The fact that the inductor is made of a conducting material such as *copper*, leads, apart from magnetic energy storage, to dissipation of heat. This property is called *winding resistance*. In addition to that, any real inductor necessarily stores electric energy which is typically described by *winding capacity*. Proper designs aims to minimize both these imperfections.

The quality of an inductor's design is typically judged by a scalar metric called *quality factor* commonly called just $Q$ [6]. In this text we will, for the sake of clarity use term Q-factor, which is a compromise between length and uniqueness. The most common definition of inductor's Q-factor is a ratio of inductor's reactance and inductor's resistance, which is equivalent to an inverse of inductor's damping factor[1].

The aim of this thesis is to study optimality of air cored inductors with respect to their Q-factor. To that point, thorough discussion of possible definitions of Q-factor is given in section 2.1.4 and in chapter 4. An important part of the thesis is also devoted to a development of fundamental bounds on inductor Q-factor which are then used the judge particular inductor designs. Proposals for design improvements are given in the end of the thesis.

[1] Damping factor reciprocal value was termed as Q-factor by Johnson in teens of the twentieth century. He says that the reason for choosing $Q$ was not the meaning of quality, but $Q$ was only one letter of the alphabet he had left since the other ones had already been pre-empted. Other interesting moments of $Q$'s history can be found in [6].

# Chapter 2

# Computational Tools

This chapter briefly introduces tools of mathematical physics used in the thesis. The first section introduces the resources necessary for the analysis of an inductor, while the second section shows basics of constrained quadratic optimization.

## 2.1 Electromagnetic Analysis

This section introduces surface electric field integral equation (EFIE) and its solution via method of moments (MoM). This results in a matrix description of electromagnetic scattering which is well prepared for optimization. This section also introduces the metric to be optimized, i.e., Q-factor of an inductor.

### 2.1.1 Surface Electric Field Integral Equation

This subsection follows [7, 8, 9] and shows the most important steps in derivation of the surface electric field integral equation (EFIE). All quantities are assumed to be Fourier's spectral densities with position vector $\boldsymbol{r}$ and angular velocity $\omega$ being their independent variables. Fourier's transform is

assumed in a form

$$\hat{\boldsymbol{F}}(\boldsymbol{r},t)=\frac{1}{2\pi}\int_{-\infty}^{\infty}\boldsymbol{F}(\boldsymbol{r},\omega)\mathrm{e}^{\mathrm{j}\omega t}\,\mathrm{d}t. \tag{2.1}$$

Since this thesis is solely focused on air-cored cored inductors, only vacuum surrounding is considered with $\epsilon_0$ denoting permittivity of vacuum and $\mu_0$ denoting permeability of vacuum.

The starting point for derivation of EFIE is the vector Helmholtz equation for magnetic vector potential $\boldsymbol{A}(\boldsymbol{r},\omega)$ [5]

$$\nabla^2\boldsymbol{A}+k^2\boldsymbol{A}=-\mu_0\boldsymbol{K}, \tag{2.2}$$

where $k=\omega\sqrt{\epsilon_0\mu_0}$ is a wavenumber and $\boldsymbol{K}(\boldsymbol{r},\omega)$ is a surface current density flowing on an infinitesimally thin metallic strip $S_{\mathrm{ms}}$. The solution to (2.2) reads [5]

$$\boldsymbol{A}(\boldsymbol{r},\omega)=\mu_0\int_{S_{\mathrm{ms}}}\boldsymbol{K}(\boldsymbol{r}',\omega)G(\boldsymbol{r},\boldsymbol{r}',\omega)\,\mathrm{d}S', \tag{2.3}$$

where $G(\mathbf{r},\mathbf{r}',\omega)$ denotes free-space Green's function,

$$G(\boldsymbol{r},\boldsymbol{r}',\omega)=\frac{\mathrm{e}^{-\mathrm{j}k|\boldsymbol{r}-\boldsymbol{r}'|}}{4\pi|\boldsymbol{r}-\boldsymbol{r}'|}. \tag{2.4}$$

The electric field produced by current density $\boldsymbol{K}$ reads

$$\boldsymbol{E}^{\mathrm{s}}(\boldsymbol{r},\omega)=-\mathrm{j}\omega\left[\boldsymbol{A}(\boldsymbol{r},\omega)+\frac{1}{k^2(\omega)}\nabla(\nabla\cdot\boldsymbol{A}(\boldsymbol{r},\omega))\right]. \tag{2.5}$$

Substituting (2.3) into (2.5), the electric field can be written as

$$\boldsymbol{E}^{\mathrm{s}}(\boldsymbol{r},\omega)=-\mathrm{j}\omega\mu_0\left[1+\frac{1}{k^2(\omega)}\nabla\nabla\cdot\right]\int_{S_{\mathrm{ms}}}\boldsymbol{K}(\boldsymbol{r}',\omega)G(\boldsymbol{r},\boldsymbol{r}',\omega)\,\mathrm{d}S'. \tag{2.6}$$

Electric field integral equation is formed by enforcing boundary condition on tangential electric field on a highly conducting surface [5], namely

$$\boldsymbol{E}^{\mathrm{i}}_{\mathrm{tan}}+\boldsymbol{E}^{\mathrm{s}}_{\mathrm{tan}}=R_{\mathrm{s}}\boldsymbol{K}, \tag{2.7}$$

where $\boldsymbol{E}^{\mathrm{i}}$ is an incident electric field and $R_{\mathrm{s}}$ is a surface resistivity [10],

$$R_{\mathrm{s}}(\omega)=\sqrt{\frac{\omega\mu}{2\sigma}}, \tag{2.8}$$

$\sigma$ is the material conductivity and $\mu$ is its permeability. Subindex $_{\tan}$ is used to isolate vector components tangential to the surface $S_{\mathrm{ms}}$. Boundary condition (2.7) is to be satisfied at $\boldsymbol{r} \in S_{\mathrm{ms}}$, i.e., over the entire conductor supporting of the current density.

Finally, EFIE can be written as

$$\boldsymbol{E}^{\mathrm{i}}_{\tan}(\boldsymbol{r},\omega) = R_{\mathrm{s}}(\omega)\boldsymbol{K}(\boldsymbol{r},\omega) + \\ + \left( \mathrm{j}\omega\mu_0 \left[ 1 + \frac{1}{k^2(\omega)} \nabla\nabla\cdot \right] \int\limits_{S_{\mathrm{ms}}} \boldsymbol{K}(\boldsymbol{r'},\omega) G(\boldsymbol{r},\boldsymbol{r'},\omega)\, \mathrm{d}S' \right)_{\tan}, \tag{2.9}$$

which is an integral equation for current density $\boldsymbol{K}$ and which must hold for $\boldsymbol{r} \in S_{\mathrm{ms}}$.

### 2.1.2 Method of Moments

In this subsection, [9, 7] is followed and method of moments (MoM) is briefly introduced. The basic idea of MoM is the reduction of operator equations to a system of linear equations which is then solved by techniques of linear algebra.

Consider an inhomogeneous linear operator equation

$$\mathcal{M}(\boldsymbol{f}) = \boldsymbol{g} \tag{2.10}$$

where $\mathcal{M}$ is a linear operator, $\boldsymbol{g}$ is known complex vector function of excitation and $\boldsymbol{f}$ is an unknown complex vector function to be determined. In order to solve (2.10), the expansion of function $\boldsymbol{f}$ into a complete set of linearly independent basis functions $\{\boldsymbol{\psi}_n\}_{n=1}^{N}$ is carried out,

$$\boldsymbol{f} = \sum_n \alpha_n \boldsymbol{\psi}_n, \tag{2.11}$$

where $\{\alpha_n\}_{n=1}^{N}$ are unknown coefficients. An example of basis function which are used in this thesis is shown in section 3.4. Substituting (2.11) in (2.10) and using the linearity of $\mathcal{M}$ yields

$$\sum_n \alpha_n \mathcal{M}(\boldsymbol{\psi}_n) = \boldsymbol{g}. \tag{2.12}$$

A set of testing functions $\{\boldsymbol{\psi}_n\}_{n=1}^{N}$, which are identical to basis functions, is now applied using a inner product,

$$\langle \boldsymbol{f}, \boldsymbol{g} \rangle = \int\limits_S \boldsymbol{f}^*(\boldsymbol{r}) \cdot \boldsymbol{g}(\boldsymbol{r}) \mathrm{d}S, \tag{2.13}$$

which is known as Galerkin method [7]. This results in

$$\sum_n \alpha_n \langle \boldsymbol{\psi}_m, \mathcal{M}(\boldsymbol{\psi}_n) \rangle = \langle \boldsymbol{\psi}_m, \boldsymbol{g} \rangle, \tag{2.14}$$

which can be written in matrix form,

$$\boldsymbol{\Upsilon} \boldsymbol{\alpha} = \boldsymbol{\chi}, \tag{2.15}$$

where $\upsilon_{mn} = \langle \boldsymbol{\psi}_m, \mathcal{M}(\boldsymbol{\psi}_n) \rangle$ and $\chi_m = \langle \boldsymbol{\psi}_m, \boldsymbol{g} \rangle$.

If basis functions are linearly independent, matrix $\boldsymbol{\Upsilon}$ is regular and expansion coefficients $\boldsymbol{\alpha}$ can be obtained as

$$\boldsymbol{\alpha} = \boldsymbol{\Upsilon}^{-1} \boldsymbol{\chi}. \tag{2.16}$$

### 2.1.3 Application of MoM to EFIE

This section shows an application of MoM to the EFIE (2.9). The EFIE is an in-homogeneous linear operator equation with linear operator

$$\mathcal{M}(\boldsymbol{K}) = R_\mathrm{s} \boldsymbol{K} + \left( \mathrm{j}\omega\mu_0 \left[ 1 + \frac{1}{k^2(\omega)} \nabla\nabla\cdot \right] \int_{S_\mathrm{ms}} \boldsymbol{K} G(\boldsymbol{r}, \boldsymbol{r'}, \omega) \, \mathrm{d}S' \right)_\mathrm{tan}, \tag{2.17}$$

with integration over the support of current density $\boldsymbol{K}(\boldsymbol{r}, \omega)$. The excitation is given by an incident electric field $\boldsymbol{E}^\mathrm{i}_\mathrm{tan}$.

Following (2.11), the surface current density is expanded as

$$\boldsymbol{K}(\boldsymbol{r}, \omega) = \sum_{n=1}^{N_{\boldsymbol{K}}} I_n(\omega) \boldsymbol{\psi}_n(\boldsymbol{r}), \tag{2.18}$$

and Galerkin testing (2.14) is performed. This results in a linear equation system,

$$(\mathbf{L} + \mathbf{Z})\mathbf{I} = \mathbf{V}. \tag{2.19}$$

with matrix elements given by

$$l_{m,n} = R_\mathrm{s} \int_{S_\mathrm{ms}} \boldsymbol{\psi}^*_m(\boldsymbol{r}) \cdot \boldsymbol{\psi}_n(\boldsymbol{r}) \, \mathrm{d}S, \tag{2.20}$$

$$z_{m,n}(\omega) = \mathrm{j}\omega\mu \int_{S_\mathrm{ms}} \boldsymbol{\psi}^*_m(\boldsymbol{r}) \cdot \left[ 1 + \frac{1}{k^2(\omega)} \nabla\nabla\cdot \right] \int_{S_\mathrm{ms}} \boldsymbol{\psi}_n(\boldsymbol{r'}) G(\boldsymbol{r}, \boldsymbol{r'}, \omega) \, \mathrm{d}S' \mathrm{d}S. \tag{2.21}$$

and with excitation vector

$$v_m(\omega) = \int\limits_{S_{\mathrm{ms}}} \boldsymbol{\psi}_m^*(\boldsymbol{r}) \cdot \boldsymbol{E}_{\tan}^{\mathrm{i}}(\boldsymbol{r}, \omega)\ \mathrm{d}S. \tag{2.22}$$

For a spatially independent surface resistivity $R_{\mathrm{s}}$, the matrix $\mathbf{L}$ can be further rewritten as $R_{\mathrm{s}}\mathbf{\Gamma}$, where $\mathbf{\Gamma}$ is the Gram matrix [11]. The elements of the impedance matrix $z_{m,n}$ can also be simplified. Using identities of vector analysis, the $\nabla\nabla\cdot$ term can be moved towards basis functions which yields

$$\begin{aligned} z_{m,n}(\omega) = \mathrm{j}\omega\mu \int\limits_{S_{\mathrm{ms}}} \int\limits_{S_{\mathrm{ms}}} \Big[ & \boldsymbol{\psi}_m^*(\boldsymbol{r}) \cdot \boldsymbol{\psi}_n(\boldsymbol{r'}) + \\ & - \frac{1}{k^2(\omega)} \nabla \cdot \boldsymbol{\psi}_m^*(\boldsymbol{r}) \nabla' \cdot \boldsymbol{\psi}_n(\boldsymbol{r'}) \Big] G(\boldsymbol{r}, \boldsymbol{r'}, \omega)\ \mathrm{d}S' \mathrm{d}S. \end{aligned} \tag{2.23}$$

an expression which is much simpler to implement [7].

Multiplying (2.19) from left by Hermitian (conjugate) transpose of $\mathbf{I}$ and comparing this formula with complex Poynting theorem [9],

$$\mathbf{I}^{\mathrm{H}} \left( \mathbf{Z} + \mathbf{L} \right) \mathbf{I} = \mathbf{I}^{\mathrm{H}} \mathbf{V}, \tag{2.24}$$

reveals that the cycle mean power lost in heat can be calculated as

$$P_{\mathrm{lost}} = \frac{1}{2} \mathbf{I}^{\mathrm{H}} \mathbf{L} \mathbf{I}, \tag{2.25}$$

the cycle mean radiated power can be calculated as

$$P_{\mathrm{rad}} = \frac{1}{2} \mathbf{I}^{\mathrm{H}} \mathbf{R} \mathbf{I}, \tag{2.26}$$

and that the cycle mean reactive power can be calculated as

$$P_{\mathrm{react}} = 2\omega(W_{\mathrm{m}} - W_{\mathrm{e}}) = \frac{1}{2} \mathbf{I}^{\mathrm{H}} \mathbf{X} \mathbf{I}, \tag{2.27}$$

where matrices $\mathbf{R}$ and $\mathbf{X}$ abbreviate real and imaginary part of matrix $\mathbf{Z}$, respectively, and $W_{\mathrm{m}}, W_{\mathrm{e}}$ stand for cycle mean magnetic and electric energy.

Another bilinear form of interest is the cycle mean stored energy [12], which can be expressed as

$$W_{\mathrm{stored}} = W_{\mathrm{m}} + W_{\mathrm{e}} = \frac{1}{4} \mathbf{I}^{\mathrm{H}} \frac{\partial \mathbf{X}}{\partial \omega} \mathbf{I} \tag{2.28}$$

which in connection with (2.27) generate expressions for cycle mean magnetic energy

$$W_{\mathrm{m}} = \frac{W_{\mathrm{stored}} + \dfrac{1}{2\omega} P_{\mathrm{react}}}{2} = \frac{1}{8} \mathbf{I}^{\mathrm{H}} \left( \frac{\partial \mathbf{X}}{\partial \omega} + \frac{\mathbf{X}}{\omega} \right) \mathbf{I} = \frac{1}{4\omega} \mathbf{I}^{\mathrm{H}} \mathbf{X}_{\mathrm{m}} \mathbf{I}, \tag{2.29}$$

and cycle mean electric energy

$$W_{\mathrm{e}} = \frac{W_{\mathrm{stored}} - \frac{1}{2\omega}P_{\mathrm{react}}}{2} = \frac{1}{8}\mathbf{I}^{\mathrm{H}}\left(\frac{\partial \mathbf{X}}{\partial \omega} - \frac{\mathbf{X}}{\omega}\right)\mathbf{I} = \frac{1}{4\omega}\mathbf{I}^{\mathrm{H}}\mathbf{X}_{\mathrm{e}}\mathbf{I}. \tag{2.30}$$

### 2.1.4 Inductor Q-factor

In most general terms, Q-factor can be defined as a ratio of desired energy contained in the device (for example magnetic energy in an inductor) and undesired energy (for example energy dissipated in heat),

$$Q = 2\pi\frac{W_{\mathrm{use}}}{W_{\mathrm{un}}}. \tag{2.31}$$

In the case of an inductor a common way is to denote magnetic energy as the desired energy, while to consider dissipated energy and radiated energy as undesired. This leads to two most commonly used Q-factors of an inductor [13], namely,

$$Q_1 = \frac{P_{\mathrm{react}}}{P_{\mathrm{rad}} + P_{\mathrm{loss}}} = \frac{\mathbf{I}^{\mathrm{H}}\mathbf{X}\mathbf{I}}{\mathbf{I}^{\mathrm{H}}(\mathbf{R}+\mathbf{L})\mathbf{I}} \tag{2.32}$$

and

$$Q_2 = \frac{2\omega W_{\mathrm{m}}}{P_{\mathrm{rad}} + P_{\mathrm{loss}}} = \frac{\mathbf{I}^{\mathrm{H}}\mathbf{X}_{\mathrm{m}}\mathbf{I}}{\mathbf{I}^{\mathrm{H}}(\mathbf{R}+\mathbf{L})\mathbf{I}}. \tag{2.33}$$

Although commonly used in practice, Q-factors (2.32) and (2.33) suffer from ignoring electric energy generated by the inductor. Considering, however, the basic functionality of an inductor, its electric energy should be considered as undesired and according to (2.31) it should appear in the denominator of Q-factor. To this point, we define Q-factor

$$Q_3 = \frac{2\omega W_{\mathrm{m}}}{P_{\mathrm{rad}} + P_{\mathrm{loss}} + \frac{\omega}{2\pi}W_{\mathrm{e}}} = \frac{\mathbf{I}^{\mathrm{H}}\mathbf{X}_{\mathrm{m}}\mathbf{I}}{\mathbf{I}^{\mathrm{H}}\left(\mathbf{R}+\mathbf{L}+\frac{1}{4\pi}\mathbf{X}_{\mathrm{e}}\right)\mathbf{I}}. \tag{2.34}$$

as an alternative to (2.32) and (2.33). Section 4.1 shows a comparison of all three definitions and a corresponding discussion.

## 2.2 Optimization

As will be shown in section 4.2, it is often interesting to ask, what the highest possible value of a given Q-factor for a given current support is (thus for given

matrices $\mathbf{R}, \mathbf{X}, \mathbf{L}, \mathbf{X}_\mathrm{e}, \mathbf{X}_\mathrm{m}$) with assumption, that current $\mathbf{I}$ can be arbitrary. In order to find such optimal Q-factor, the quadratically constrained quadratic program [14, 15] is defined in this section and its solution via application of Lagrange multipliers is also shown.

### 2.2.1 Quadratically Constrained Quadratic Program

All inductor Q-factors defined in section 2.1.4 are written as a ratio of bilinear forms

$$\frac{\mathbf{I}^\mathrm{H}\mathbf{A}\mathbf{I}}{\mathbf{I}^\mathrm{H}\mathbf{B}\mathbf{I}}, \tag{2.35}$$

where $\mathbf{A}$, $\mathbf{B}$ are, at least in principle, positive definite matrices [16]. In order to maximize inductor Q-factor, optimization problem

$$\max_{\mathbf{I}} \frac{\mathbf{I}^\mathrm{H}\mathbf{A}\mathbf{I}}{\mathbf{I}^\mathrm{H}\mathbf{B}\mathbf{I}} \tag{2.36}$$

must be solved. This problem is equivalent to a quadratically constrained quadratic program [14, 15],

$$\max_{\mathbf{I}} \mathbf{I}^\mathrm{H}\mathbf{A}\mathbf{I}, \qquad \text{subject to} \qquad \mathbf{I}^\mathrm{H}\mathbf{B}\mathbf{I} = 1,\ \mathbf{A} \succ 0,\ \mathbf{B} \succ 0. \tag{2.37}$$

### 2.2.2 Solution via Lagrange Multipliers

This subsection introduces the Lagrange multipliers method [14, 15], which is used to solve (2.37).

Lagrange function corresponding to a single constrained optimization (2.37) reads [14, 15]

$$\mathcal{L}(\mathbf{I}, \lambda) = \mathbf{I}^\mathrm{H}\mathbf{A}\mathbf{I} - \lambda(\mathbf{I}^\mathrm{H}\mathbf{B}\mathbf{I} - 1) = \mathbf{I}^\mathrm{H}(\mathbf{A} - \lambda\mathbf{B})\mathbf{I} + \lambda, \tag{2.38}$$

where $\lambda$ is so-called Lagrage multiplier. The theory of constrained optimization then proves, that stationary points of Lagrange function are also stationary points of the original optimization problem. In order to find these stationary points, a complex gradient operator [17] is applied to (2.38) which leads to

$$0 = \tilde{\nabla}_{\mathbf{I}^*}\mathcal{L}(\mathbf{I}, \lambda) = (\mathbf{A} - \lambda\mathbf{B})\mathbf{I}. \tag{2.39}$$

The stationary points of Lagrange function (2.38) have thus solutions to a generalized eigenvalue problem

$$\mathbf{A}\mathbf{I} = \lambda\mathbf{B}\mathbf{I} \tag{2.40}$$

The eigenvectors of (2.40) are defined up to a multiplication constant, therefore it can be assumed that normalization

$$\mathbf{I}^{\mathrm{H}}\mathbf{B}\mathbf{I} = 1. \tag{2.41}$$

is enforced. This normalization also implies that optimization constraint (2.37) is satisfied at all stationary points. If (2.40) is left multiplied by $\mathbf{I}^{\mathrm{H}}$ and normalization (2.41) is used, the maximized quadratic form reduces to

$$\mathbf{I}^{\mathrm{H}}\mathbf{A}\mathbf{I} = \lambda \tag{2.42}$$

in every stationary point. This implies that the solution to (2.37) is given by the largest eigenvalue of (2.40).

### 2.2.3 Maximization of Q-factor

When methods of setion 2.2.2 are applied to Q-factors defined in section 2.1.4, their maximum attainable values can be evaluated. Taking $\mathbf{A} = \mathbf{X}_{\mathrm{m}}$ and $\mathbf{B} = \mathbf{R} + \mathbf{L} + \mathbf{X}_{\mathrm{e}}/(4\pi)$ as an example, section 2.2.2 claims that the highest eigenvalue of the generalized eigenvalue problem

$$\mathbf{X}_{\mathrm{m}}\mathbf{I} = \lambda\left(\mathbf{R} + \mathbf{L} + \frac{1}{4\pi}\mathbf{X}_{\mathrm{e}}\right)\mathbf{I}. \tag{2.43}$$

corresponds to the maximum value of Q-factor $Q_3$.

# Chapter 3

# Discretization of Inductor Structures

This chapter contains description of structures used to model inductors. Section 3.1 introduces triangularization and its implementation in MATLAB® [18], subsequent sections 3.2, 3.3 show meshes which are used in this study. RWG functions [8], which are employed as basis and testing functions within MoM, are introduced in section 3.4.

## 3.1 Mesh Generation Tools

In order to use RWG basis functions, a triangular mesh of the described surface is needed. This section introduces two software tools written in MATLAB® [18]. The first is a strip mesh generator[1], which is used to generate triangular mesh of strips build along arbitrary parametric curves in three dimensions which describe windings of studied inductors. The second is AToM which is used for triangularization of patches and to build basis functions.

[1]The strip mesh generator was developed by the author of the thesis. Owing to its unique capabilities, it will, in a future release, become a part of Antenna Toolbox for MATLAB (AToM) [19] package, an electromagnetic simulation tool developed at the department of electromagnetic field at CTU FEE Prague.

### 3.1.1 Strip Mesh Generator

Strip mesh generator assumes a strip created along a predefined curve in three dimensional space. The curve is described by its parametrization, which is accompanied by a chosen width and normal vector to the plane of the strip. The curve creates the central line of the strip. The triangularization begins with a longitudinal segmentation of the strip into a user defined number of trapezoids. Finally, triangles are created by division of these trapezoids.

Apart from a user defined parametrization, this tool includes a list of predefined strip structures which are shown in section 3.3 as triangularized inductor structures. An example of a particular realization is shown in figure 3.1. An example of a user-defined parametrization of a strip is shown

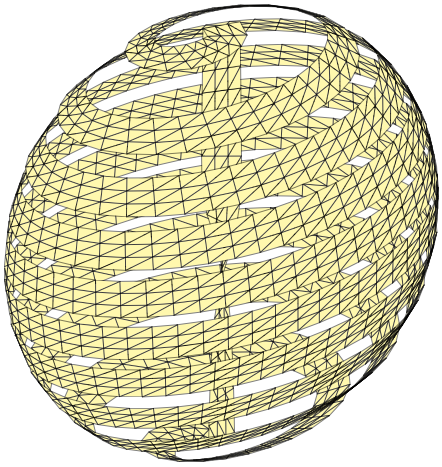

**Figure 3.1:** An example of an ellipsoidal helix.

in listing 3.1. This particular parametrization generates strip plotted in figure 3.2.

**Listing 3.1:** Example of a parametric strip to be meshed as defined in MATLAB® [18].

```
%% def
a=2;
b=3;
c=2*pi;

% required
points=@(x) [a*cos(c*x), b*sin(c*x), 0*x]; % curve
along=@(x) [-c*a*sin(c*x), c*b*cos(c*x), 0*x]; % curve derivation
normal=@(x) [0*x-1, 0*x, 1+0*x]; % vector perpendicular to vector
                                 %  perpendicularly traversing the strip
width=@(x) 0.5*(1+8*(x-0.5).^2); % width of strip

% optional
ind.Ncells=2; % trapezoids per strip width
ind.Npoints=20; % number of curve points
```

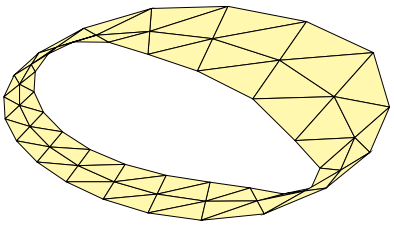

**Figure 3.2:** The result of a parametric strip defined in listing 3.1.

## 3.2 Meshes for Evaluation of Bounds

This section shows surfaces which are used for evaluation of fundamental bounds on Q-factor of an inductor. The following surfaces are taken into account:

1. a cylinder,
2. an ellipsoid,
3. a torus,
4. a circle,
5. a rectangle.

All these canonical surfaces can be seen as supports for realizable inductors introduced in section 3.3, namely: cylindrical helix, ellipsoidal helix, toroidal helix, circular spiral and rectangular spiral.

The discretization of a circle and a rectangle has been performed in AToM. Triangularizations of a sphere and a cylinder have been made using an in-house code provided by Miloslav Čapek.

Triangularization of torus has been made by a MATLAB code prepared for this thesis. To that point, a triangularized planar square patch [1 mm × 1 mm] is prepared with square pixels each consisting of two triangles. Nodes of triangles are afterwards mapped onto the torus by a vector function of two parameters,

$$\boldsymbol{r}(t_1,t_2) = \begin{bmatrix} (a - h\cos(2\pi t_1))\cos(2\pi t_2) \\ (b - h\cos(2\pi t_1))\sin(2\pi t_2) \\ h\sin(2\pi t_1) \end{bmatrix}, \quad t_1, t_2 \in [0,1]\,, \tag{3.1}$$

where $[a, b]$ are toroidal semi-axes and $h$ is the radius of the torus tube.

## 3.3 Mesh for Realizable Inductors

Real inductor structures corresponding to their canonical supports introduced in section 3.2 are presented in this section. Following structures are prepared:

1. Cylindrical helix,

$$\boldsymbol{r}(t) = \begin{bmatrix} a\cos(2\pi f t + \varphi) \\ b\sin(2\pi f t + \varphi) \\ h(t - 0.5) \end{bmatrix}, \quad t \in [0, 1], \tag{3.2}$$

where $[a, b]$ are $x$ and $y$ semi-axes of cylindrical base, $h$ is the height of the helix, $f$ is the number of turns and $\varphi$ is the cylindrical angular variable. A particular example of a cylindrical helix is shown in figure 3.3.

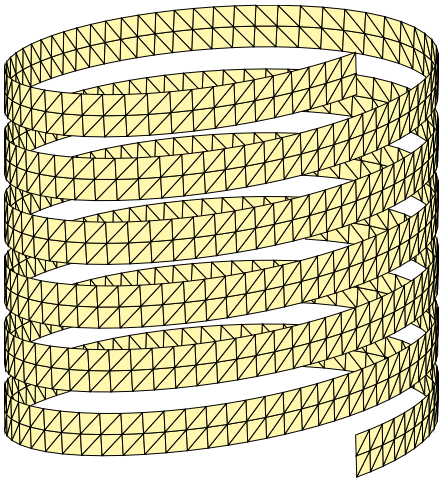

**Figure 3.3:** Meshed cylindrical helix.

2. Ellipsoidal helix,

$$\boldsymbol{r}(t) = \begin{bmatrix} a\sqrt{1 - 4(t - 0.5)^2}\cos(2\pi f t + \varphi) \\ b\sqrt{1 - 4(t - 0.5)^2}\sin(2\pi f t + \varphi) \\ h(t - 0.5) \end{bmatrix}, \quad t \in [0, 1], \tag{3.3}$$

where $[a, b]$ are $x$ and $y$ ellipsoid semi-axes and all other parameters are the same as for cylindrical helix. A particular example of an ellipsoidal helix is shown in figure 3.1.

3. The parametrization of a toroidal helix, with a representative example shown in figure 3.4, reads

$$\boldsymbol{r}(t) = \begin{bmatrix} [a - h\cos(2\pi f t + \varphi)]\cos(2\pi t) \\ [b - h\cos(2\pi f t + \varphi)]\sin(2\pi t) \\ h\sin(2\pi f t + \varphi) \end{bmatrix}, \quad t \in [0, 1], \tag{3.4}$$

where $[a, b]$ are $x$ and $y$ ring semi-axis, $h$ is the radius of torus tube, $f$ number of turns and $\varphi$ is the tube angular variable.

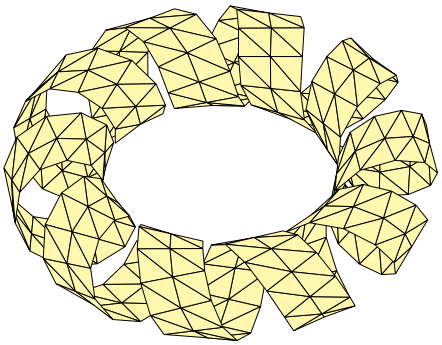

**Figure 3.4:** Meshed toroidal helix.

4. Parametrizations of linear and logarithmic spiral are shown in the following.

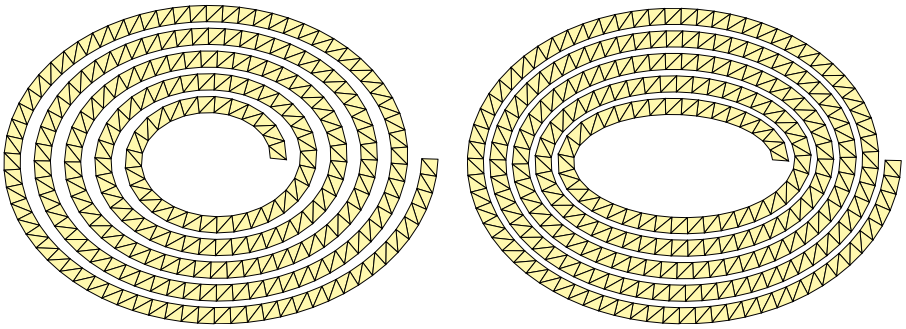

**(a) :** Classical linear spiral. **(b) :** Equidistant gap linear spiral.

**Figure 3.5:** Comparison of the classical and the equidistant gap linear spiral.

- Classical linear spiral,

$$\boldsymbol{r}(t) = \begin{bmatrix} a(t(1-h)+h)\cos(2\pi f t+\varphi) \\ b(t(1-h)+h)\sin(2\pi f t+\varphi) \\ 0 \end{bmatrix}, \quad t \in [0,1], \tag{3.5}$$

  where $[a, b]$ are the outer semi-axes and $h$ is the ratio of inner and outer semi-axis. Particular example is shown in the left panel of figure 3.5.

- Equidistant gap linear spiral,

$$\boldsymbol{r}(t) = \begin{bmatrix} (b(1-h)(t-1)+a)\cos(2\pi f t+\varphi) \\ b(t(1-h)+h)\sin(2\pi f t+\varphi) \\ 0 \end{bmatrix}, \quad t \in [0,1],\ a > b. \tag{3.6}$$

  Inequality $a > b$ makes the function dual in $x$ and $y$ axes. Particular example is shown in the right panel of figure 3.5.

- Parametrization of a logarithmic spiral, with a particular example shown in figure 3.7, reads

$$\boldsymbol{r}(t) = \begin{bmatrix} a\mathrm{e}^{bt}\cos(2\pi f t + \varphi) \\ a\mathrm{e}^{bt}\sin(2\pi f t + \varphi) \\ 0 \end{bmatrix}, \quad t \in [0, 1], \tag{3.7}$$

  where $a$ is the radius in the beginning of the spiral and $b$ is the factor controlling exponential growth of the spiral.

5. Rectangular spiral, with a representative example shown in figure 3.6. The parametrization of a rectangular spiral contains a loop over piecewise defined functions and it is thus not shown explicitly. The parameters controlling this parametrization are outer edge length in $x$ and $y$ direction which are denoted as $a$ and $b$, number of turns $f$ and ratio between the inner and outer edge length which is denoted as $h$.

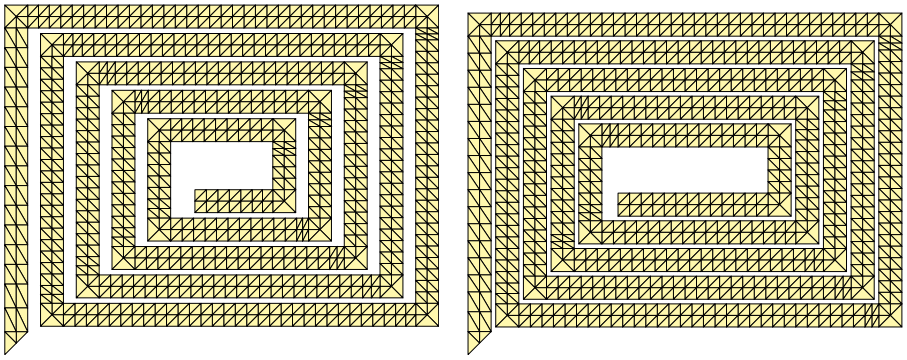

**(a) :** Classical rectangular spiral. **(b) :** Equidistant gap rec. spiral.

**Figure 3.6:** Comparison of the classical and the equidistant gap rectangular spiral.

In order to form inductors from strips defined in this section, a meshed connection between the beginning and the end of the strip is needed (An exception being toroidal helix which already forms a closed loop). This connection has been implemented for all parametrization discussed above. An example of the connection bridge in the case of a logarithmic spiral is shown in figure 3.7.

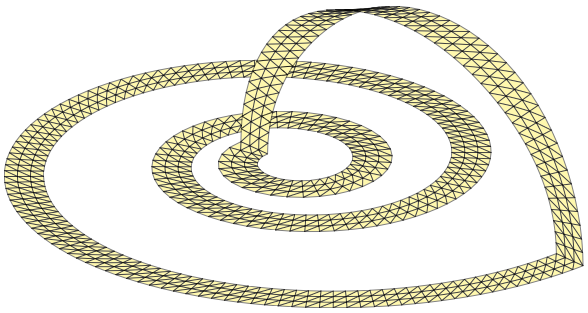

**Figure 3.7:** Meshed logarithmic spiral with a bridge forming a closed galvanically connected loop.

## 3.4 Basis and Testing Functions

In this section, Rao-Wilton-Glisson (RWG) triangular functions[2] [8] are introduced. Within this thesis, RWG functions are used as basis and testing functions in MoM solution to EFIE which was shown in section 2.1.3.

An RWG function is defined for a triangular mesh as follows,

$$\boldsymbol{\psi}_n(\boldsymbol{r}) = \begin{cases} \dfrac{L_n}{2A_n^+}\boldsymbol{\rho}_n^+(\boldsymbol{r}), & \boldsymbol{r} \in T_n^+ \\ \dfrac{L_n}{2A_n^-}\boldsymbol{\rho}_n^-(\boldsymbol{r}), & \boldsymbol{r} \in T_n^- \\ 0, & \text{otherwise}, \end{cases} \tag{3.8}$$

where $T_n^+$ and $T_n^-$ is a pair of adjacent triangles sharing a common edge $e_n$ with length $L_n$. The geometrical representation of used parameters is shown in figure 3.8. Vector $\boldsymbol{\rho}_n^+(\boldsymbol{r})$ is oriented towards the vertex $\mathbf{V}_n^+$, i.e.,

$$\boldsymbol{\rho}_n^+(\boldsymbol{r}) = \mathbf{V}_n^+ - \boldsymbol{r}; \quad \boldsymbol{r} \in T_n^+, \tag{3.9}$$

while, vector $\boldsymbol{\rho}_n^-(\boldsymbol{r})$ points away from the vertex $\mathbf{V}_n^-$, i.e.,

$$\boldsymbol{\rho}_n^-(\boldsymbol{r}) = \mathbf{V}_n^- - \boldsymbol{r}; \quad \boldsymbol{r} \in T_n^-. \tag{3.10}$$

The elements of impedance matrix $\mathbf{Z}$ (2.23) indicates the necessity of evaluation of the basis function divergence. Its computation can be performed

[2] RWG function is the most commonly used basis function in MoM solution to EFIE since its introduction in 1982 [7].

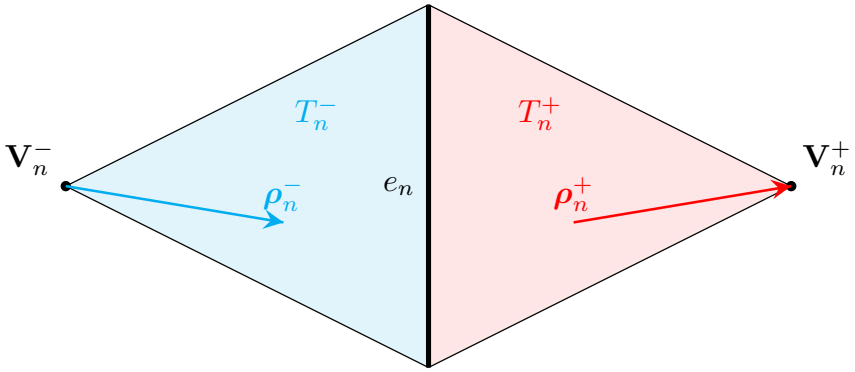


**Figure 3.8:** Illustration of RWG function.

by using cylindrical coordinate system with $\mathbf{V}_n^+$ or $\mathbf{V}_n^-$ at the origin [7]. This results in

$$\nabla \cdot \boldsymbol{\psi}_n(\boldsymbol{r}) = \begin{cases} \dfrac{-L_n}{A_n^+}, & \boldsymbol{r} \in T_n^+ \\ \dfrac{L_n}{A_n^-}, & \boldsymbol{r} \in T_n^- \\ 0, & \text{otherwise.} \end{cases} \tag{3.11}$$

The final form of matrix elements (2.20) and (2.23) is reached by substituting (3.8) and (3.11) to appropriate relations. Computation of all mentioned matrices with RWG functions is implemented in AToM [20].

### 3.4.1 Antenna Toolbox for MATLAB

Antenna Toolbox for MATLAB (AToM) [19] presents a unique tool for analysis and synthesis of planar electromagnetic structures which is being developed at the department of electromagnetic field at CTU FEE in Prague[3]. The most significant functionality of AToM used in this thesis is the evaluation of matrices introduced in section 2.1.3. AToM furthermore offers a feeding via delta gap voltage source which is used to excite realistic inductors. Lastly, this thesis extensively uses plots of surface current density which were made by plotting tools of AToM.

[3] Author of the thesis is a member of AToM's development team.

# Chapter 4

# Results

This chapter shows the major findings of this thesis. Particular realization of inductors are assessed in section 4.1. Performance of these inductors is then compared with the corresponding fundamental bounds in section 4.2. Lastly, section 4.3 proposes and tests inductor modifications for Q-factor enhancement.

## 4.1 Realizable Inductors

Realizable inductors are addressed first and their performance is compared based on Q-factor definitions given in section 2.1.4. All evaluations in this section are carried out for surface resistivity $R_s = 0.01\ \Omega$, that approximately models a copper strip at frequency 1.4 GHz [10, 21]. The particular value of the used surface resistivity is however of low significance, since all presented results are normalized such as to minimize its effect. The normalized Q-factor used in this chapter reads

$$\frac{R_s Q}{Z_0 ka}, \tag{4.1}$$

where electrical size $ka$ is used instead of angular frequency $\omega$, with $a$ being the radius of the smallest sphere circumscribing the structure [22]. The impedance of vaccum used in (4.1) is defined as [23] $Z_0 = \sqrt{\mu_0/\epsilon_0}$. At small electrical sizes $ka \to 0$, where all Q-factors defined in section 2.1.4 asymptotically behaves as $Q \to \omega L/R$, where $L$ is the self-inductance of the inductor and $R$ is the resistance of the inductor, it can be observed that normalization (4.1) provides quantity that is independent of material, frequency and number of

turns of the underlying inductor. This normalized Q-factor can thus, at small electrical sizes, be used as an absolute metric judging how the particular shape of an inductor (planar spiral, cylindrical helix, etc.) affects the Q-factor.

As examples, the normalized Q-factors of inductors formed by a cylindrical helices with radii 0.5 mm, heights 1 mm, six and three turns, strip widths 0.13 mm and 0.24 mm, are shown in figure 4.2. The surface current densities evaluated at electrical size $ka = 10^{-3}$ are shown in figure 4.1.

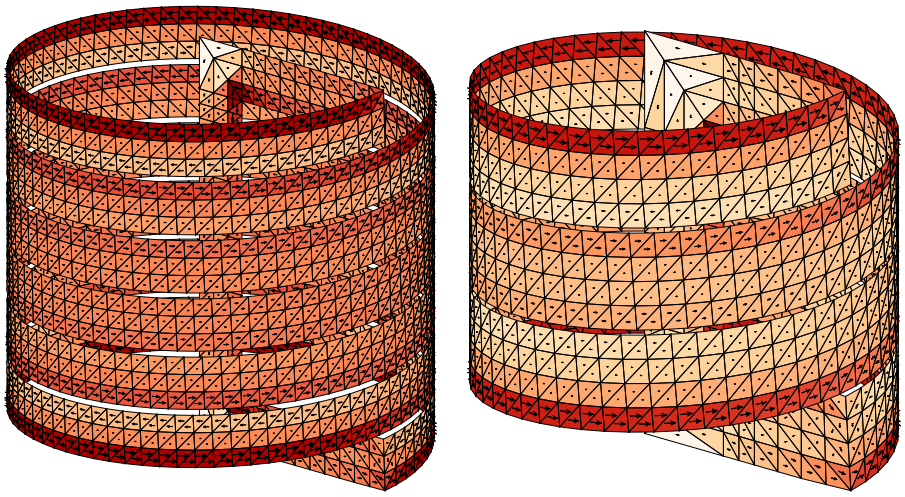

**(a) :** With 6 turns. **(b) :** With 3 turns.

**Figure 4.1:** Current density on cylindrical helices for $ka = 10^{-3}$.

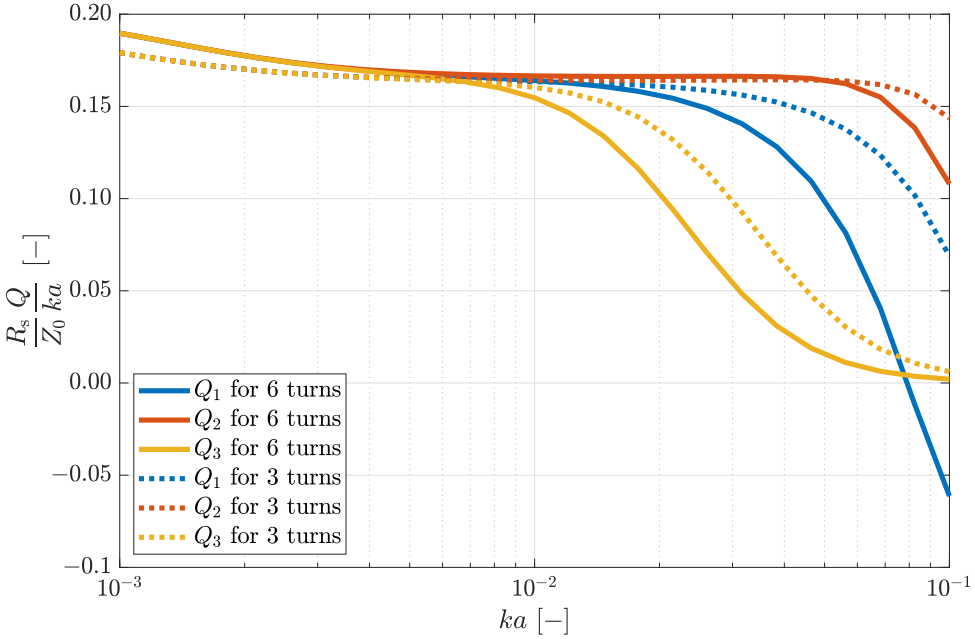


**Figure 4.2:** Q-factor of cylindrical helices shown in figure 4.1.

Figure 4.2 shows that cycle mean radiated and electric energy is negligible at small electrical sizes and that depicted normalized Q-factors are just weakly dependent on frequency. In contrast, when electrical size is higher, and inter-turn capacities starts the store considerable amount of electric energy, the three definitions of Q-factor posed in section 2.1.4 start to behave differently. Particularly, the Q-factor $Q_1$ starts to suffer from the vicinity of the resonance of the inductor and stops to show the "quality" of an inductor. The same is true for Q-factor $Q_2$ which also does not penalize electric energy. Due to these drawbacks, only Q-factor $Q_3$ is used in the rest of the result section.

Another important thing which confirms figure 4.2 is that Q-factors does not significantly depend on number of turns. The reason for this behaviour is that, on the one hand, if the number of turns is increased, the self inductance is also increased, but on the other hand, the strip is lengthened, which causes more significant energy dissipation in heat.

Collecting the above mentioned observations, the normalized Q-factors of all realizable inductors studied in this thesis are shown in figure 4.3, their parameters are in table A.1 and current densities in figures A.1a – A.5a.

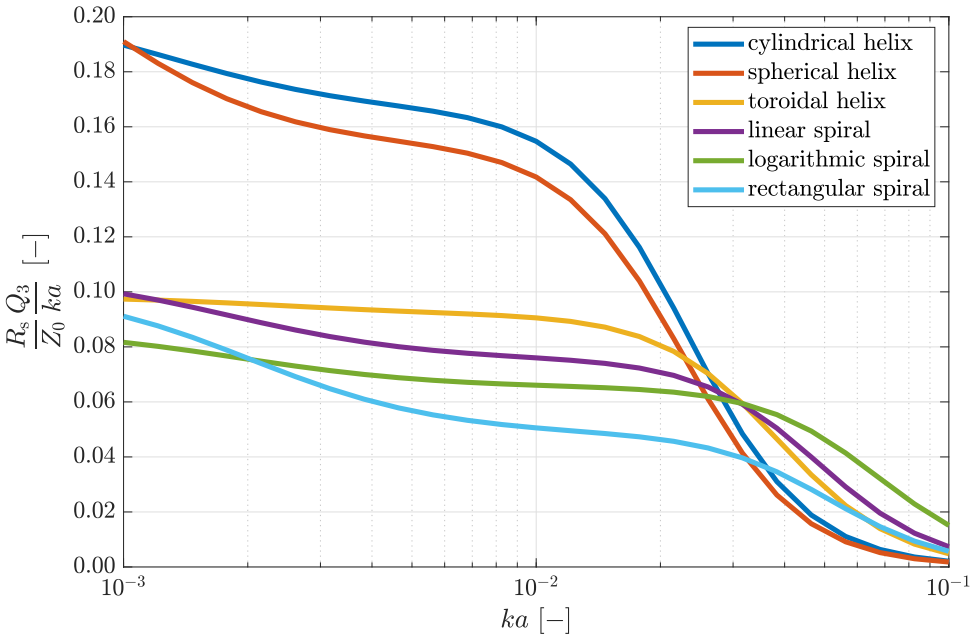


**Figure 4.3:** Comparison of Q-factors of different inductor structures.

For the chosen metric of Q-factor $Q_3$ (2.34), the figure clearly indicates that the best performance is provided by inductors in a form of cylindrical and spherical helix. Q-factors of all planar inductors is considerably worse, the best (linear spiral) being almost twice lower in Q-factor than volumetric

inductors. A notable exception from this rule is a toroidal helix, whose Q-factor is poor. The reason for this behavior is explained in next section.

## 4.2 Bounds

Fundamental bounds on Q-factor gives the highest possible Q-factor that can be realized with a given current support. Therefore, if a Q-factor of an inductor is compared to a fundamental bound corresponding to its support, the result shows how effectively the realized inductor uses the given shape. In addition, the normalization by a fundamental bound also removes material and frequency dependencies since the fundamental bound on Q-factor and the Q-factor of a realized inductor are evaluated for the same material.

In this thesis, the fundamental bound on Q-factor is evaluated according to section 2.2.3. The task of finding the largest eigenvalue of the underlying generalized eigenvalue problem is solved via build-in MATLAB® [18] function as shown in listing 4.1.

**Listing 4.1:** Q-factor $Q_3$ eigenvalue problem implementation in MATLAB® [18].

```
[Ivec,QoptList(1,ika)] = eigs(Xmmat,(Rmat+Lmat+Xemat/(4*pi)),1,'la'); % bound
```

In this way a fundamental bound on Q-factor has been found for all surfaces described in section 3.2. The optimal current densities can be seen in figures A.1b – A.5b, the proportions of canonical structures correspond to realized inductors in table A.1. The fundamental bounds of Q-factor generated by these optimal currents were subsequently used to normalize Q-factor from figure 4.3. These normalized curves are plotted in figure 4.4.

The comparison depicted in figure 4.4 qualitatively differs from that shown in figure 4.3 and offers several important observations:

- Except for the cylindrical helix, all inductors do not use the given current support effectively, the most notable example being toroidal helix, where optimal current density dramatically differs from current density on toroidal helix.
- The best current support for an inductor with respect to a Q-factor is given by a sphere, while the worst is given by a rectangle.

- With no exception, the efficiency of magnetic energy storage decreases rapidly with increasing electrical size.

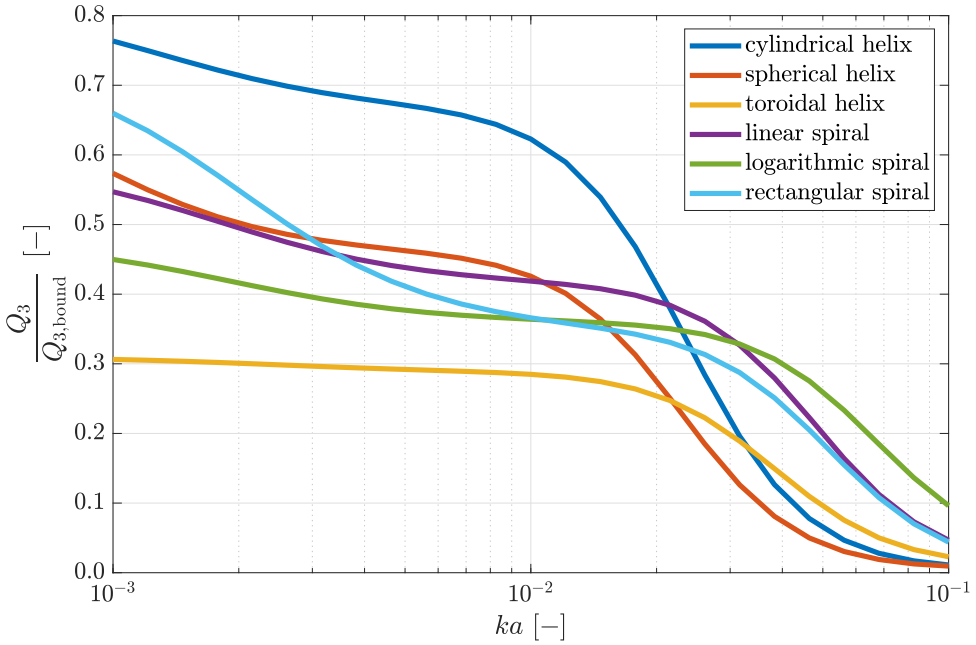


**Figure 4.4:** Comparison of Q-factors of realized inductors with Q-factor bounds.

## 4.3 Inductor Modifications for Q-factor Enhancement

The aim of this section is to modify realized inductors in order to mitigate some of the deficiencies discussed in previous section. To address this, an attempt is made to modify inductor strip such as to better approximate the current density defining the fundamental bound. In addition, an interesting question could be asked, is dependence of fundamental bound on proportions of underlying structure?

The first modification concerns the cylindrical helix. Figure A.1b shows a surface current density of an optimal current existing on a cylindrical surface while the current existing on a realized cylindrical helix inductor is shown in A.1a. Clearly, the fundamental bound suggests that current density should be maximized in the central part of cylinder and minimized on the top and bottom of the cylinder. To approach this a modified parametrization of the

cylindrical helix is proposed

$$\boldsymbol{r}(t) = \begin{bmatrix} \mathrm{a}\cos(2\pi f t + \varphi) \\ \mathrm{b}\sin(2\pi f t + \varphi) \\ \mathrm{c}\dfrac{(t\sqrt[3]{4} - \sqrt[3]{0.5})^3 + t - 0.5}{2} \end{bmatrix}, \quad t \in [0, 1]\,, \tag{4.2}$$

where parameters are the same entities as in the original parametrization of the cylindrical helix. Furthermore, strip width is also defined by a parametric function,

$$w(t) = w_0(4(1-d)t^2 + 4(d-1)t + 1), \quad t \in [0, 1]\,, \tag{4.3}$$

where $w_0$ is the width of the strip at the beginning and end of the helix, while $d$ describes a ration of strip width in the beginning of the helix and the strip width at the center of the cylinder. Particular parameters can be found in table A.1.

The current density on the modified cylindrical helix is shown in figure A.6a. Visually, the current density resembles that of the fundamental bound better. Unfortunately, this modification actually worsened the Q-factor as can be seen from figure 4.5, the reason most probably being the increased ohmic losses in the central region of the helix. A question on an optimal parametrization of a cylindrical helix with which the realizable Q-factor will attain its highest possible value thus remains opened.

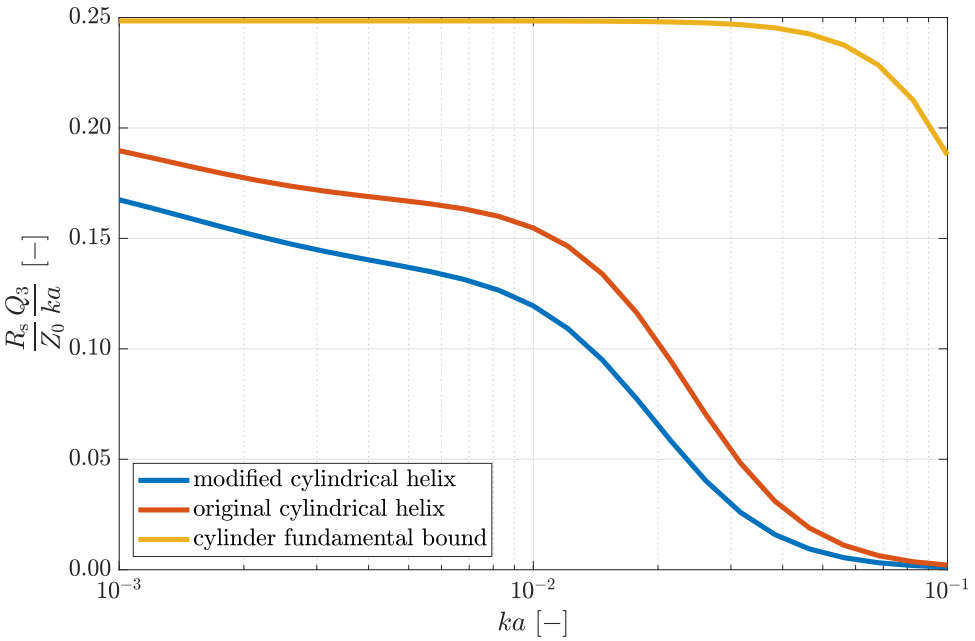


**Figure 4.5:** Q-factor comparison of the modified cylindrical helix from figure A.6a and of the original cylindrical helix. The Q-factor corresponding to the fundamental bound is also shown.

Contrary to cylindrical helix, if linear spiral was considered as a modification of a logarithmic spiral, the Q-factor would be increased. This might imply that the optimal physically realizable inductor is reached by a structure with a constant strip width and equidistant gap between inductor turns. This hypothesis can easily be tested on a spherical helix which does not show an equidistant gap. Would the Q-factor be increased, if the spherical helix was drawn with equidistant gap between strips? The new parametrization of a spherical helix reads

$$\boldsymbol{r}(t) = \begin{bmatrix} a\sin(\pi t)\cos(2\pi f t + \varphi) \\ b\sin(\pi t)\sin(2\pi f t + \varphi) \\ -\dfrac{c}{2}\cos(\pi t) \end{bmatrix}, \quad t \in [0,1]\,. \tag{4.4}$$

The answer to the question of Q-factor change is unclear, because the modification decreases Q-factor at smaller electrical sizes $ka$, while increases Q-factor at higher electrical sizes, which can be seen from figure 4.6. It is also important to mention that comparing with the fundamental bound, this change is minor. Current density on the modified spherical helix[1] is plotted in figure A.6b and particular parameters used in the evaluation can be found in table A.1.

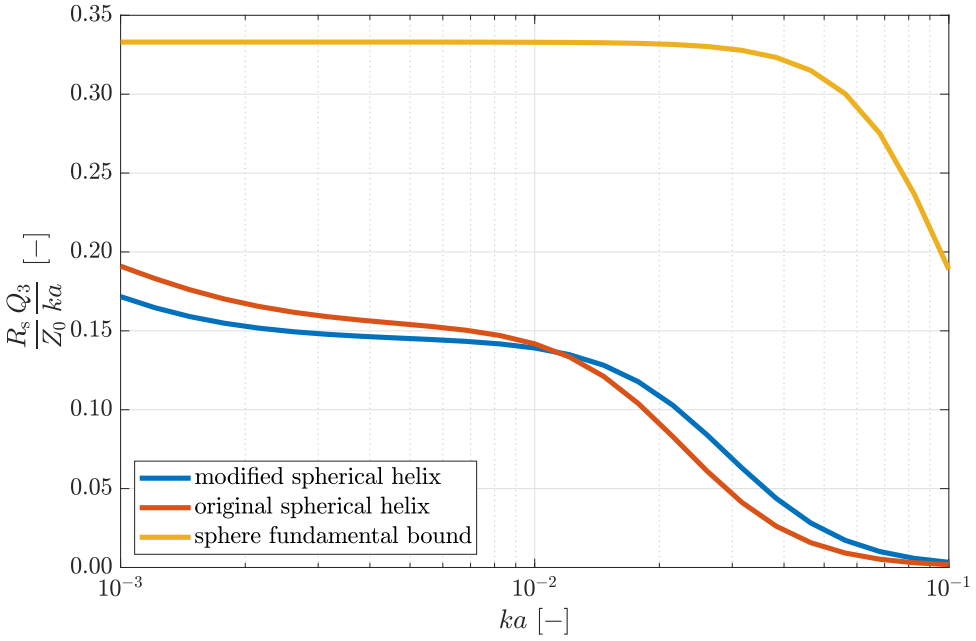


**Figure 4.6:** Q-factor comparison of the modified spherical helix from figure A.6a and of the original spherical helix. The Q-factor corresponding to the fundamental bound is also shown.

The inductor modifications, which applied in order to increase its Q-factor,

[1] In this particular realization, the strip does not terminate on the $z$ axis, because the curvature near this axis is immense, which invalidates mesh by triangles overlap.

has been unsuccessful a decreases it. This implies the difficulty of geometrical optimization. It indicates a necessity of physical understanding of effects decreasing the Q-factor of realistic inductors. Future work would be focused on this topic.

Another interesting question touched upon this section is a dependence of fundamental bound on proportions of underlying structure. In this respect, only the Q-factor bound of a sphere is universal. In the case of say cylinder, it is not clear what the best ratio of cylinder's diameter to its length which would maximize Q-factor bound is? In order to find an answer, golden section search method [24, 25] has been applied to this optimization task. The resulting optimal ratio[2] of cylinder's diameter to its length is 1.26. The fundamental bound on Q-factor of a cylinder for a varying ratio of diameter and length is plotted in figure 4.7.

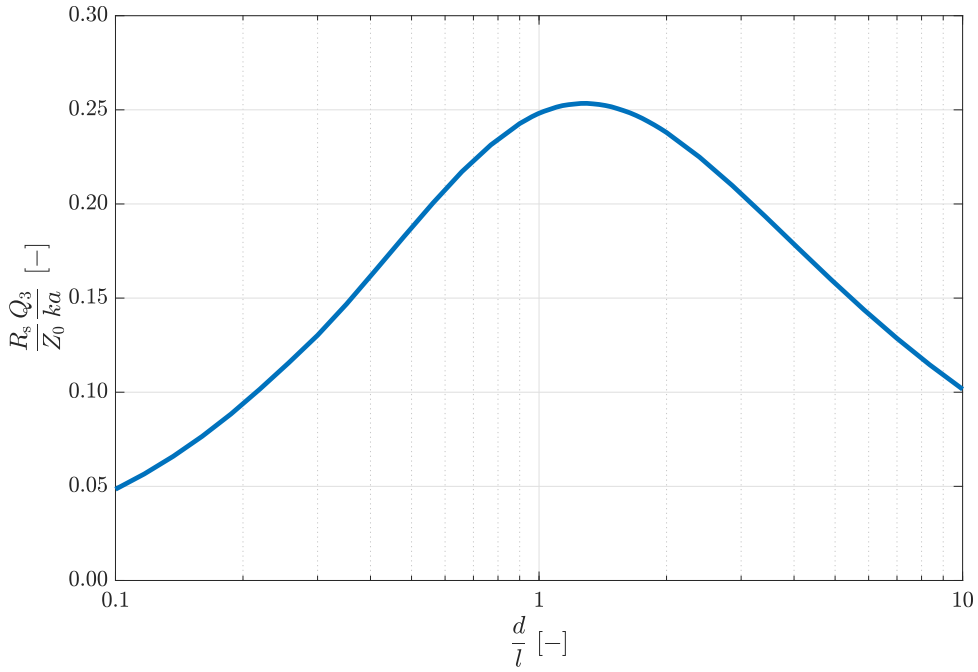


**Figure 4.7:** Q-factor bound of a cylinder in dependence on cylinder's diameter $d$ and length $l$ for $ka = 10^{-3}$.

[2] As a further work, two dimensional golden section search [25] could be applied to find the optimal strip width and number of turns for the found optimal ratio in an effort to reach probably the best cylindrical helix inductor.

# Chapter 5

# Conclusion

The aim of the thesis was to get acquainted with quality factor of air cored inductors and the way of their computation and optimization. The task was divided into individual steps.

Firstly, the computational tools of mathematical physics such as surface electric field integral equation (EFIE), method of moments (MoM) and quadratic programming were introduced and subsequently used to evaluate Q-factor of an inductor. Quadratically constrained quadratic program was used to find fundamental bounds of provided Q-factors.

Second, tools for generating triangular mesh of common inductor structures were developed.

Lastly, Q-factors of common air-cored inductors were evaluated and compared with corresponding fundamental bounds. This induced several important questions with respect to the improvement of realizable inductors. Geometric optimizations attempts to achieve this improvement were unsuccessful.

Future work would be focused on triangularization of parametric surfaces. The idea is to transform the surface from a three dimensional space to a plane, mesh it in two dimensional space and subsequently map the mesh back to three dimensions. The triangularization should be done with respect to surface parameter derivatives, which give relation between distance in plane and in original surface, to ensure better quality of mapped mesh. This

idea has been already applied to triangularization of torus. Another field of interest for future work would be geometrical optimization of inductors. Of primary importance in this task is a physical understanding of what effects degrades the performance of realistic inductors when compared to corresponding fundamental bounds. Finally, an interesting field of study concerns Q-factor bound in presence of volumetric current densities.

# Appendix A

## Current densities

This appendix contains current densities on structures used in chapter 4, inductor's parameters are stated in table A.1.

| Inductor struct. | Fig. | $a$ [mm] | $b$ [mm] | $h$ [-,mm] | $f$ [-] | $\varphi$ [rad] | $w$[1] [mm] |
|---|---|---|---|---|---|---|---|
| Cylindrical helix[2] | A.1a | 0.50 | 0.50 | 0.87 | 6 | 0 | 0.13 |
| Spherical helix | A.2a | 1.00 | 1.00 | 1.00 | 7 | 0 | 0.30 |
| Toroidal helix | A.3a | 2.00 | 2.00 | 1.00 | 12 | 0 | 0.50 |
| Linear spiral[3] | A.4a | 0.88 | 0.88 | 0.15 | 4 | 0 | 0.12 |
| Logarithmic spir.[4] | A.4b | 0.20 | 1.55 | - | 3 | 0 | 0.12 |
| Rectangular spir. | A.5a | 1.00 | 1.00 | 0.20 | 5 | - | 0.07 |
| Modified cyl. h.[5] | A.6a | 0.50 | 0.50 | 0.83 | 7 | 0 | [0.05,0.17] |
| Modified sph. h. | A.6b | 1.00 | 1.00 | 1.00 | 7 | 0 | 0.40 |

**Table A.1:** Parameters of the realized inductors.

[1] $w$ is the width of strip.

[2] Cylindrical helix's total high is $h + w = 1$ mm.

[3] Linear spiral total outer radius is 1 mm.

[4] Logarithmic spiral total outer radius is $ae^b + w/2 \doteq 1$ mm.

[5] Modified cylindrical helix's total high is $h + w_0 = 1$ mm and its width $w(t)$ is in the interval for all $t \in [0, 1]$.

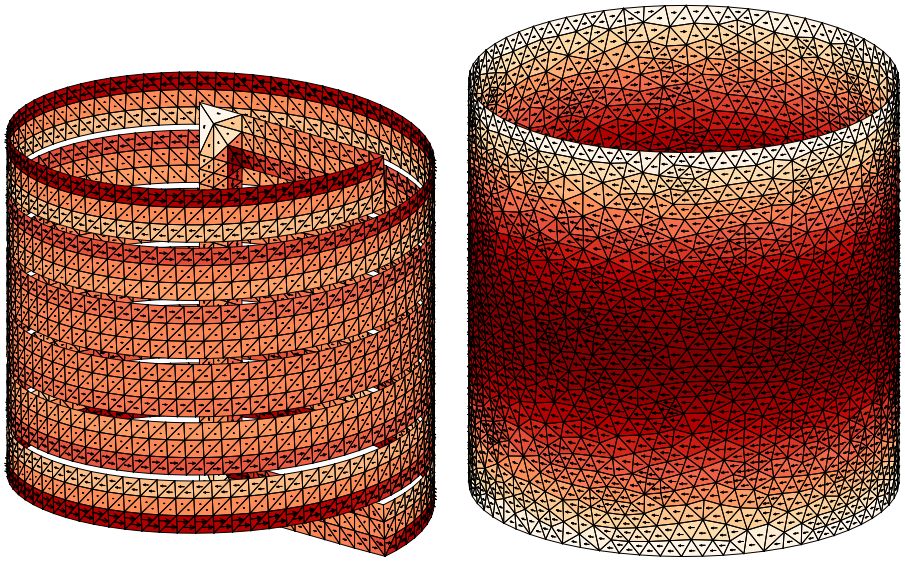

**(a) :** Cylindrical helix. **(b) :** Bound.

**Figure A.1:** Current density on a cylinder for $ka = 10^{-3}$.

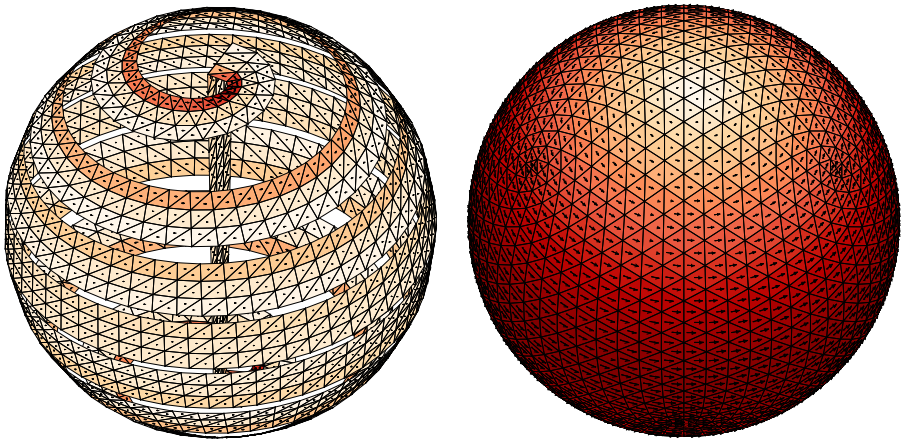

**(a) :** Spherical helix. **(b) :** Bound.

**Figure A.2:** Current density on a sphere for $ka = 10^{-3}$.

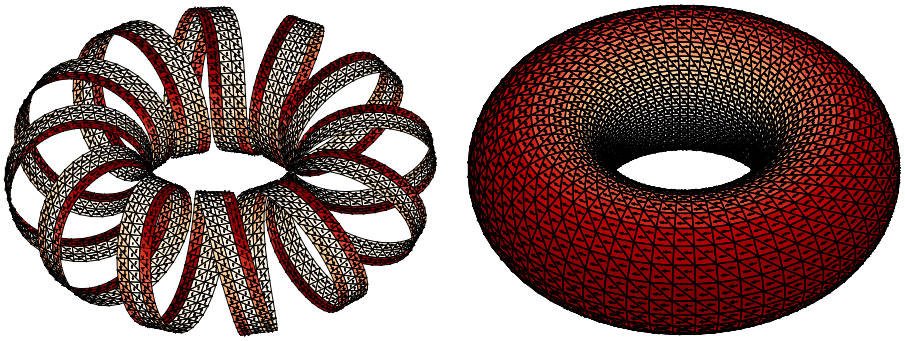

**(a) :** Toroidal helix. **(b) :** Bound.

**Figure A.3:** Current density on a torus for $ka = 10^{-3}$.

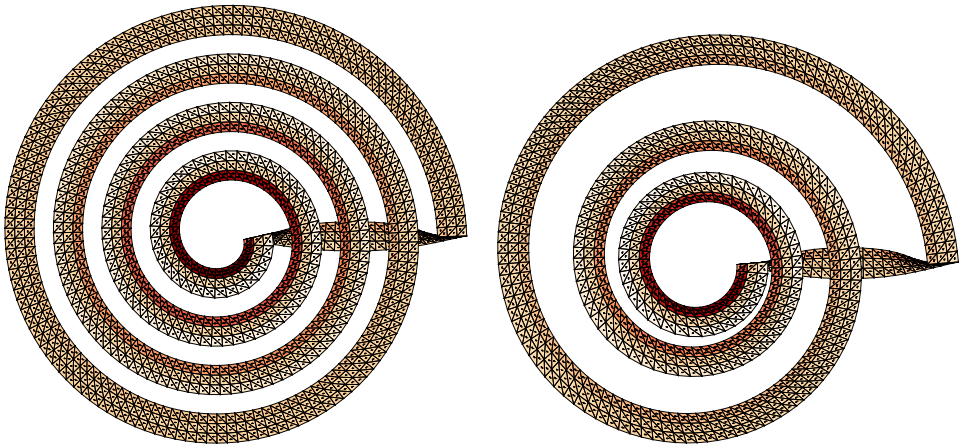

**(a) :** Linear spiral. **(b) :** Logarithmic spiral.

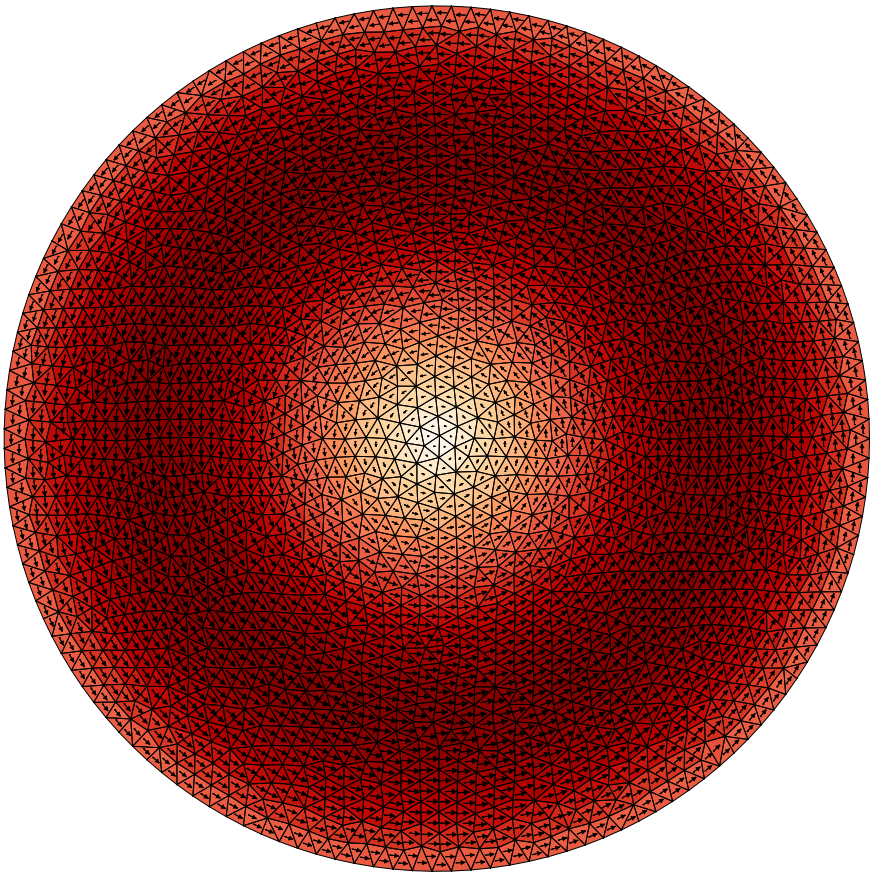

**(c) :** Bound.

**Figure A.4:** Current density on a circle for $ka = 10^{-3}$.

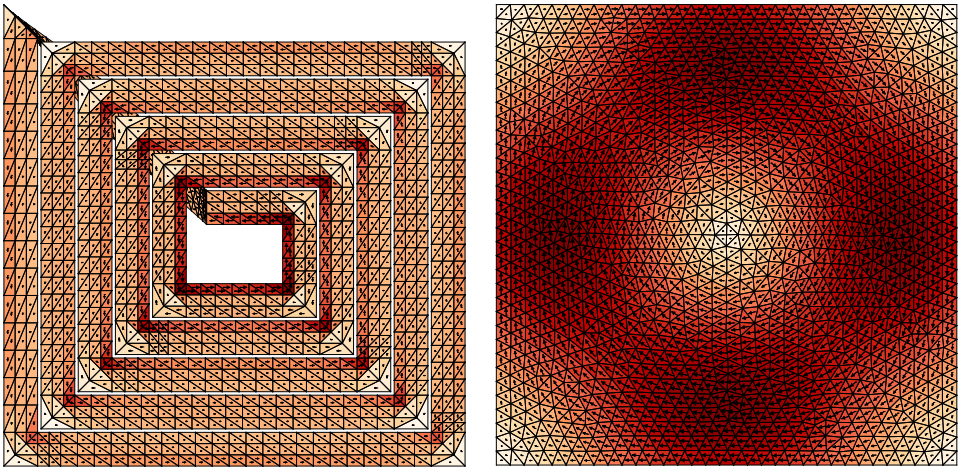

**(a) :** Rectangular spiral. **(b) :** Bound.

**Figure A.5:** Current density on a rectangle for $ka = 10^{-3}$.

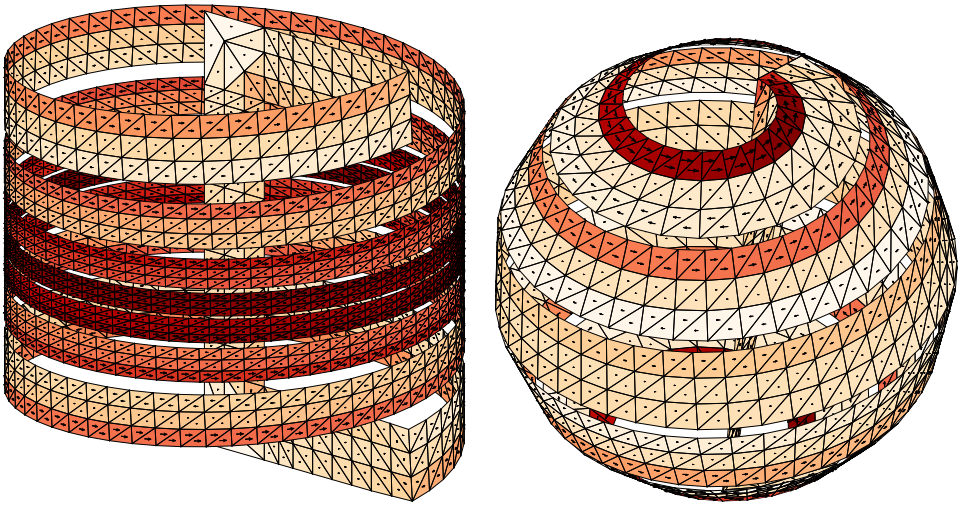

**(a) :** Modified cylindrical helix. **(b) :** Modified spherical helix.

**Figure A.6:** Current density on modified helices for $ka = 10^{-3}$.

# Appendix B

# Provided MATLAB Functions and Scripts

## B.1 Important Functions and Scripts

- strip2mesh\mesh.strip_mesh.m generates triangular mesh along a strip defined point by point, an example of its use is shown in strip2mesh\pbp_def.m.
- strip2mesh\own_parametric_strip.m generates triangular mesh along a strip defined by parametric functions, an example of its use is shown in strip2mesh\parametric.m, which is shown in listing 3.1.
- strip2mesh\curve_strip_to_mesh.m generates triangular mesh along predefined strips, which are shown in section 3.3, an example of its use is shown in strip2mesh\disp_strip.m.
- strip2mesh\toroid.m generates triangular mesh on a toroid.
- inductor_Qfactor.m computes all defined Q-factors for realizable inductor structures and Q-factor $Q_3$ bound for corresponding structure. The triangular meshes and position of delta gap voltage supply are prepared in mat-files. Figures 4.2 – 4.6 have been created by combination of its outputs.
- cyl_opt.m computes the Q-factor $Q_3$ fundamental bound accordingly to the cylinder's ratio of diameter and length, subsequently it generates the chart in figure 4.7.
- cyl_opt_gold.m computes optimal ratio of cylinder's diameter to its length by golden section search method [24, 25], whose result is in section 4.3.

## B.2 Content of CD-ROM

- strip2mesh
  - +curves
    - +specifications
      - bridge_generator.m
      - curve_control.m
      - curve_definitions.m
      - curve_step.m
      - equidistant_parameter.m
    - cylindrical_helix.m
    - linear_spiral.m
    - logarithmic_spiral.m
    - rectangular_spiral.m
    - spherical_helix.m
    - toroidal_helix.m
  - +mesh
    - mesh_correction.m
    - strip_mesh_generator.m
  - +utilities
    - norm_row.m
  - curve_strip_to_mesh.m
  - own_parameteric_strip.m
  - disp_strip.m
  - parametric.m
  - pbp_def.m
  - toroid.m
- cyl_opt_fun.m
- cyl_opt.m
- cyl_opt_gold.m
- inductor_Qfactor.m
- cylinder.mat
- cylinder3turns.mat
- linear.mat

- logarithmic.mat
- modCyl.mat
- modSph.mat
- rectangle.mat
- sphere.mat
- torus.mat

# Appendix C

# Bibliography


[1] C. K. Alexander and M. N. O. Sadiku, *Fundamentals of electric circuits*. McGraw-hill Education, 2017.

[2] Y. Singh, *Electromagnetic field theory*. Pearson Education India, 2011.

[3] Alibaba.com, "High precision miniature inductor coil for tv and camera [photo]." [Online; accessed from `https://is.alicdn.com/img/pb/859/856/326/326856859_550.jpg` April 30, 2019].

[4] Amazon.uk, "Toroid core inductor wire wind wound 220uh 59mohm 4a coil [photo]." [Online; accessed from `https://images-na.ssl-images-amazon.com/images/I/81kUCiCN09L._SX425_.jpg` April 30, 2019 ].

[5] J. David Jackson, *Classical Electrodynamics, 3rd Edition*. Wiley-IEEE Press, 07 1998.

[6] E. I. Green, *The Story of Q*, vol. 43. American Scientist, 1955.

[7] W. C. Gibson, *The Method of Moments in Electromagnetics*, vol. 1. CRC Press/Taylor & Francis, second ed., 2015.

[8] S. M. Rao, D. R. Wilton, and A. W. Glisson, "Electromagnetic scattering by surfaces of arbitrary shape," *Antennas and Propagation, IEEE Transactions on*, vol. 30, pp. 409 – 418, 06 1982.

[9] R. F. Harrington, *Field Computation By Moment Method*. Wiley-IEEE Press, 01 1993.

[10] E. C. Jordan and K. G. Balmain, *Electromagnetic waves and radiating systems*. Prentice-Hall, 1968.

[11] R. A Horn and C. R Johnson, *Matrix analysis, second edition*. Cambridge University Press, 01 2013.

[12] R. Harrington, "Antenna excitation for maximum gain," *IEEE Transactions on Antennas and Propagation*, vol. 13, pp. 896–903, nov 1965.

[13] O. Kenneth, "Estimation methods for quality factors of inductors fabricated in silicon integrated circuit process technologies," *Phase-Locking in High-Performance Systems*, vol. 33, p. 1249–1252, Aug 2009.

[14] S. Boyd, *Convex optimization*. Cambridge University Press, 2004.

[15] J. Nocedal and S. J. Wright, *Numerical Optimization*. Springer, 01 2006.

[16] D. Tayli, M. Capek, L. Akrou, V. Losenicky, L. Jelinek, and M. Gustafsson, "Accurate and efficient evaluation of characteristic modes," *IEEE Transactions on Antennas and Propagation*, vol. 66, no. 12, pp. 7066–7075, 2018.

[17] D. Brandwood, "A complex gradient operator and its application in adaptive array theory," *Microwaves, Optics and Antennas, IEE Proceedings H*, vol. 130, pp. 11–16, 03 1983.

[18] MATLAB, "version 9.6.0.1099231 (R2019a) Update 1," 2019. [Online; `http://https://www.mathworks.com/products/matlab.html` accessed May 17, 2019].

[19] M. Čapek, V. Adler, P. Kadlec, M. Marek, M. Štumpf, M. Mašek, V. Losenický, M. Štrambach, P. Hazdra, L. Jelínek, and et al., "Antenna Toolbox for MATLAB (AToM): A Versatile MATLAB Tool for Antenna Synthesis," 2018. [Online; `http://www.antennatoolbox.com` accessed May 17, 2019].

[20] M. Čapek, V. Adler, P. Kadlec, M. Marek, M. Štumpf, M. Mašek, V. Losenický, M. Štrambach, P. Hazdra, L. Jelínek, and et al., "AToM Documentation," Apr 2019. [Online; `http://antennatoolbox.com/download_file?file=AToM_documentation.pdf` accessed May 17, 2019].

[21] M. Ohring, *Engineering materials science*. Academic Press, 1995.

[22] R. C. James, *Mathematics dictionary*. Chapman & Hall, 5 ed., 1992.

[23] A. Zangwill, *Modern electrodynamics*. Cambridge University Press, 2013.

[24] W. H. Press, *Numerical recipes: the art of scientific computing*. Cambridge University Press, 2007.

[25] Y.-C. Chang, "N-dimension golden section search: Its variants and limitations," in *2009 2nd International Conference on Biomedical Engineering and Informatics*, IEEE, 2009.

# ZADÁNÍ BAKALÁŘSKÉ PRÁCE

## I. OSOBNÍ A STUDIJNÍ ÚDAJE

Příjmení: **Liška** Jméno: **Jakub** Osobní číslo: **466385**

Fakulta/ústav: **Fakulta elektrotechnická**

Zadávající katedra/ústav: **Katedra radioelektroniky**

Studijní program: **Otevřené elektronické systémy**

## II. ÚDAJE K BAKALÁŘSKÉ PRÁCI

Název bakalářské práce:

**Optimální činitel jakosti vzduchových induktorů**

Název bakalářské práce anglicky:

**Optimal Quality Factor of Air Cored Inductors**

Pokyny pro vypracování:

Nastudujte definici činitele jakosti induktoru a následně ji implementujte v nástroji AToM s pomocí dostupných maticových operátorů, tj. impedanční matice, matice uložené energie, a matice pro vodivostní ztráty. Výpočet ověřte pro induktory tvořené tenkými dobře vodivými pásky ve vakuu a porovnejte s výsledky v referenční literatuře. Zaměřte se na kanonické struktury (planární spirála, cylindrická šroubovice, sférická šroubovice, toroidní šroubovice), pro tyto struktury rovněž vytvořte nástroj na tvorbu triangulární mřížky z křivky předepsané analyticky. V další části práce stanovte fundamentální limity činitele jakosti pro oblasti plně zahrnující v předchozím analyzované struktury, tj. disk, válec, kouli, a toroid. Porovnejte nalezená optima s činitelem jakosti reálných struktur a proveďte tvarovou optimalizaci s ohledem na jejich vylepšení.
Školitel specialista: Doc. Ing. Miloslav Čapek, Ph.D.

Seznam doporučené literatury:

[1] R. F. Harrington, Field Computation by Moment Methods, Wiley –IEEE Press, 1993.
[2] S. M. Rao, D. R. Wilton, and A. W. Glisson, “Electromagnetic scattering by surfaces of arbitrary shape,” IEEE Transaction on Antennas and Propagation, Vol. 30, pp. 409 – 418, 1982.
[3] Square Air Core Inductors, Coilcraft, Document 720-2, 2015.
[4] H. Nagaoka, “The inductance coefficients of solenoids,” Journal of the College of Science, Vol. 27, pp. 1 – 33, 1909.
[5] J. Nocedal and S. Wright, Numerical Optimization, New York, Springer, 2006.

Jméno a pracoviště vedoucí(ho) bakalářské práce:

**doc. Ing. Lukáš Jelínek, Ph.D., katedra elektromagnetického pole FEL**

Jméno a pracoviště druhé(ho) vedoucí(ho) nebo konzultanta(ky) bakalářské práce:

Datum zadání bakalářské práce: **01.02.2019** Termín odevzdání bakalářské práce: **24.05.2019**

Platnost zadání bakalářské práce: **20.09.2020**

| doc. Ing. Lukáš Jelínek, Ph.D. | prof. Mgr. Petr Páta, Ph.D. | prof. Ing. Pavel Ripka, CSc. |
|---|---|---|
| podpis vedoucí(ho) práce | podpis vedoucí(ho) ústavu/katedry | podpis děkana(ky) |

## III. PŘEVZETÍ ZADÁNÍ

Student bere na vědomí, že je povinen vypracovat bakalářskou práci samostatně, bez cizí pomoci, s výjimkou poskytnutých konzultací. Seznam použité literatury, jiných pramenů a jmen konzultantů je třeba uvést v bakalářské práci.

. Datum převzetí zadání

Podpis studenta

 